RSC Advances

PAPER

View Article Online
View Journal | View Issue

Cite this: *RSC Adv.*, 2017, **7**, 50087

Co_3O_4 nanoparticles/MWCNTs composites: a potential scaffold for hydrazine and glucose electrochemical detection†

Tuantuan Zhou,[a] Wanlin Gao,[a] Yanshan Gao,[a] Qiang Wang *[a] and Ahmad Umar*[bc]

Received 2nd October 2017
Accepted 23rd October 2017

DOI: 10.1039/c7ra10892c

rsc.li/rsc-advances

We report the successful formation of cobalt oxide (Co_3O_4) nanoparticles/multi-walled carbon nanotubes (Co_3O_4/MWCNTs) composites as efficient electrocatalytic materials for chemical sensing. Co_3O_4/MWCNTs composites were synthesized *via* a straightforward hydrothermal treatment and comprehensively characterized. Working as effective electron mediators, the prepared Co_3O_4/MWCNTs composites were used for the fabrication of hydrazine (N_2H_4) and glucose sensors. The electrochemical impedance spectroscopy (EIS) studies confirmed Co_3O_4/MWCNTs/glassy carbon electrode (GCE) exhibited higher conductivity than bare GCE and Co_3O_4/GCE, endorsing a faster electron transfer rate and a higher electrocatalytic activity. The addition of MWCNTs can not only improve the dispersion of Co_3O_4 nanoparticles but also facilitate the electron transfer rate. The sensitivity, selectivity, repeatability, reproducibility, linear range and detection limit of the fabricated sensors were systematically investigated. The fabricated hydrazine sensor displayed a great sensitivity of 120.26 μA mM^{-1}, a wide linear range of 1.0–187.4 μM, and a rather low detection limit of 0.449 μM, and the fabricated glucose sensor exhibited a high sensitivity of 63.27 μA mM^{-1}, a wide linear range of 1.70–554 μM, and a low detection limit of 0.95 μM. We demonstrated that such fabricated Co_3O_4/MWCNTs composites may have favorable applications in the establishment of fast and effective determination of environmental pollutants.

1. Introduction

Transition metal oxides with specific structures have aroused considerable interest for their typical physicochemical properties and compositions. Some transition metal oxides, for instance, SnO_2, MnO_2, and ZnO have been widely used in electrochemical fields.[1,2] Lou *et al.*[3] reported the coaxial SnO_2 nanosphere for lithium storage. The prepared materials had a high capacity of 500 mA h g^{-1} and stable cyclability. Gao *et al.*[4] reported the MnO_2 nanoplate for supercapacitor. The fabricated supercapacitor could be reversibly cycled in a wide potential window of 0–2.0 V and exhibited a power density of 1.0 kW kg^{-1} and an energy density of 23.2 W h kg^{-1}. Freire *et al.*[5] reported the ZnO nanoparticles for electrocatalytic oxidation of phenolic compounds. The synthesized catalytic material demonstrated excellent electrochemical performances. Among various transition metal oxides, cobaltosic oxide (Co_3O_4), a type of significant transition-metal oxide semiconductors with direct optical band gaps at 2.19 eV,[6] has received intensive concern in electrochemical applications for its unique properties, such as high efficiency, environmental benign nature, nontoxicity, easy to synthesize, and so on. In recent years, Co_3O_4 based nanomaterials have been widely applied in catalysts, supercapacitors, lithium batteries, and sensors.[7–10] Xu *et al.*[11] reported Co_3O_4 nanorod in anion-exchange membrane fuel cells for oxygen reduction process. Xia *et al.*[12] and Wang *et al.*[13] synthesized Co_3O_4 nanowires arrays and coralloid Co_3O_4 for supercapacitor, respectively. Eom *et al.*[14] reported 2D porous Co_3O_4 nanofoils for lithium battery application. Li *et al.*[15] constructed peanut-like Co_3O_4 for ethanol and carbon monoxide sensing. However, although there has been extensive research on Co_3O_4 materials, the practical application of Co_3O_4 nanostructures as electrode materials remains less utilized for their low electronic conductivities and easy aggregation.[16] An effective method to enhance the conductivity and simultaneously improve the dispersibility is to introduce carbon materials as support materials. MWCNTs, functioned as extremely favorable support materials, make itself an outstanding support material for electrocatalysts with enhanced specific surface area, awesome electron conductivity, excellent chemical inertness and comparatively superior oxidation stability.[17] Multi-walled carbon nanotubes have unique hollow, intertwined network structure, which benefits the migration of electrolyte ion and

[a]*College of Environmental Science and Engineering, Beijing Forestry University, 35 Qinghua East Road, Haidian District, Beijing 100083, P. R. China. E-mail: qiang.wang.ox@gmail.com; qiangwang@bjfu.edu.cn; Tel: +86 13699130626*

[b]*Department of Chemistry, College of Science and Arts, Najran University, Najran-11001, Kingdom of Saudi Arabia. E-mail: ahmadumar786@gmail.com*

[c]*Promising Centre for Sensors and Electronic Devices (PCSED), Najran University, Najran-11001, Kingdom of Saudi Arabia*

† Electronic supplementary information (ESI) available. See DOI: 10.1039/c7ra10892c

provides more binding sites, compared with other carbon-based materials, such as graphene, activated carbon, and single-walled carbon nanotube.[18] Metal oxides entangled with MWCNTs hybrid materials have been reported in electrochemical fields. Tang *et al.* synthesized MnO_2/MWCNTs and used them for supercapacitors.[19] Wang *et al.* utilized Co_3O_4@MWCNT nanocable and Co_3O_4@MWCNT hybrid as electrode materials for supercapacitors. The addition of MWCNTs indeed enhanced the performances compared with the pristine metal oxides.[20,21]

In the monitoring of environmental pollutants, traditional methods like colorimetry,[22] spectrophotometry,[23] flow injection spectrophotometry,[24] liquid and gas chromatography[25] are complicated, high cost, and narrow linear ranges. Therefore, facile and effective analytical approaches capable of tracing the concentration of chemicals are always required. Up to date, the electrochemical method has been considered to be promising because of their cost-effectiveness, increased efficiency, high sensitivity, and ease of operation. The electrochemical behavior of chemicals is susceptible to the electrode surface structure. One problem for most electrodes is the large over-potentials during the direct oxidation of chemicals.[26] The electrooxidation of chemicals on glassy carbon electrodes shows slow kinetics due to its high over-potentials.[27] To overcome this drawback and simultaneously accelerate the electron transfer rate, some transition metal oxides like Co_3O_4 can be utilized for the optimization of the electrode surface.

At present, the development of hydrazine and glucose sensors is of great significance in a wide range of applications, particularly in environmental monitoring, energy conversion, blood glucose testing, and pharmaceutical analysis.[28–32] Therefore, in this paper Co_3O_4 nanostructures and MWCNTs were both use as the electrode materials for the formation of hydrazine and glucose sensor. The results showed that the fabricated hydrazine sensor achieved such a high sensitivity of 120.26 μA mM^{-1}, which is higher than the reported Co_3O_4/MWCNTs based sensor in hydrazine detection.

2. Experimental

2.1 Fabrication of Co_3O_4/MWCNTs composites

All commercial reagents were purchased of analytical grade and utilized directly without further purification. Before the synthesis of Co_3O_4/MWCNTs composites, the MWCNTs (HGCF-300, outer diameter *ca.* 8–13 nm and average length *ca.* 8–13 μm) were functionalized using concentrated HNO_3 by heating at 80 °C for 4 h with continuous stirring and rinsed with DI water until pH reached 7. The Co_3O_4/MWCNTs composites were fabricated through the following procedures. Firstly, 48 mg of the pretreated MWCNTs were dispersed in 52.8 mL water–ethanol mixture (the volume ratio of water to ethanol was 1 : 10) with ultrasonication for 30 min. Then 0.145 g cobalt acetate tetrahydrate was added in the above-mentioned solution. After another ultrasonic treatment for 30 min, 1.4 mL ammonia aqueous solution (25 wt%) was dropped into the solution with continuous stirring. Finally, the well-dispersed solution was constantly stirred at 80 °C for 10 h and further hydrothermally treated at 150 °C for 3 h. The obtained sample was rinsed with ethanol and water successively, and subsequently dried in the oven at 80 °C for 5 h to attain the final product. For comparison, the pure Co_3O_4 nanoparticles were also fabricated in the same way without MWCNTs.

2.2 Electrode preparation

Prior to test, the glassy carbon electrode (GCE) was polished sequentially with 1.0, 0.3 and 0.05 μm alumina powder, respectively, and carefully washed using deionized water and ethanol thoroughly before use. The Co_3O_4/MWCNTs/GCE was attained by dropping 5 μL of the Co_3O_4/MWCNTs composite dispersion (5 mg mL^{-1}) onto the pure GCE surface, and an infrared lamp was used to evaporate the residual solvent.

2.3 Samples characterisation

X-ray diffraction (XRD) spectra were explored on a Shimadzu XRD-7000 diffractometer in the 2θ range of 10–70° using Cu Kα radiation with a scanning rate of 2° min^{-1}. Transmission electron microscopy (TEM) images were gained by JEOL JEM 2100. Field-emission scanning electron microscopy (FESEM) images of samples were acquired on JEOL JSM-6701F microscope. N_2 adsorption–desorption isotherms were measured on a Bulider SSA-7000 system, and the sample was degassed at 220 °C for 4 h before the test. Raman spectrum was examined by Renishaw inVia in the range of 200–2000 cm^{-1}. Electrochemical experiments were carried out on a CHI660e electrochemical workstation (CH Instruments Company, Shanghai, China) using a conventional three-electrode system. The modified glassy carbon electrode ($\Phi = 3$ mm) served as the working electrode, while the platinum wire and saturated calomel electrode were adopted as the counter and reference electrodes, respectively.

3. Results and discussion

3.1 Characterisations of Co_3O_4/MWCNTs composites

Fig. 1(a) shows the wide-angle XRD patterns of MWCNTs, Co_3O_4 and Co_3O_4/MWCNTs composites. The oxidized MWCNTs with a strong diffraction peak at $2\theta = 26.58$ is ascribed to the (002) reflection of graphitic carbon (JCPDS card: no. 41-1487). Additionally, other three weak peaks appeared at $2\theta = 37.84$, 43.98, 64.32, respectively, are corresponding to the peaks of the aluminium sample holder (PDF standard card no. 04-0787). In addition, all of these three peaks have a 0.8 degree left shift, compared with the standard card, because of the concave surface of sample holder. The signals appeared on the MWCNTs pattern are resulted from the low density of MWCNTs, the X-ray penetrates the MWCNTs powder. When mixed with Co_3O_4, the high density of Co_3O_4 prevents the X-ray from being penetrating, so that the signals disappeared on the Co_3O_4/MWCNTs composites. The Co_3O_4/MWCNTs composites exhibited eight obvious diffraction peaks which are in coincidence with the standard cubic Co_3O_4 (JCPDS card: no. 43-1003) as well as one characteristic peak of MWCNTs. The average size can be calculated from the (311) peak with Scherrer equation.

$$D_c = K\lambda/\beta \cos\theta \quad (1)$$

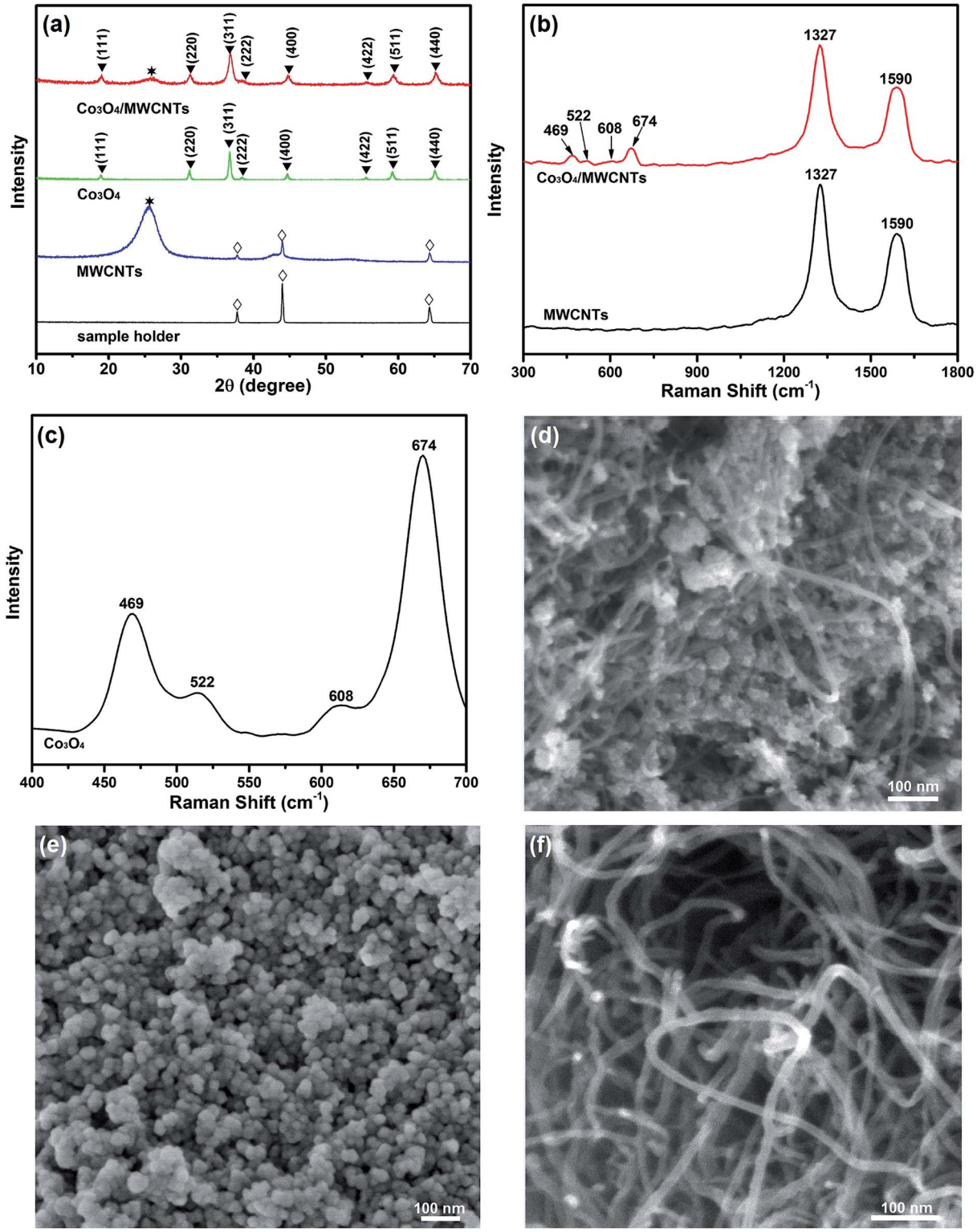

Fig. 1 (a) XRD spectra of MWCNTs, Co_3O_4 and Co_3O_4/MWCNTs composites, (b) room temperature Raman spectra of the MWCNTs and Co_3O_4/MWCNTs composites, (c) room temperature Raman spectra of bare Co_3O_4 particles (d) FE-SEM image of Co_3O_4/MWCNTs composites, (e) FE-SEM image of Co_3O_4 particles and (f) FE-SEM image of MWCNTs.

where K refers to a constant (*ca.* 0.9), λ represents the X-ray wavelength (0.1542 nm), θ is the Bragg angle, and β refers to the full width at half maximum in radiations, *i.e.* the broadening caused by the crystallite dimensions. The diameter of Co_3O_4 nanoparticle turns out to be 10.2 nm. These results indicated that the Co_3O_4/MWCNTs composites

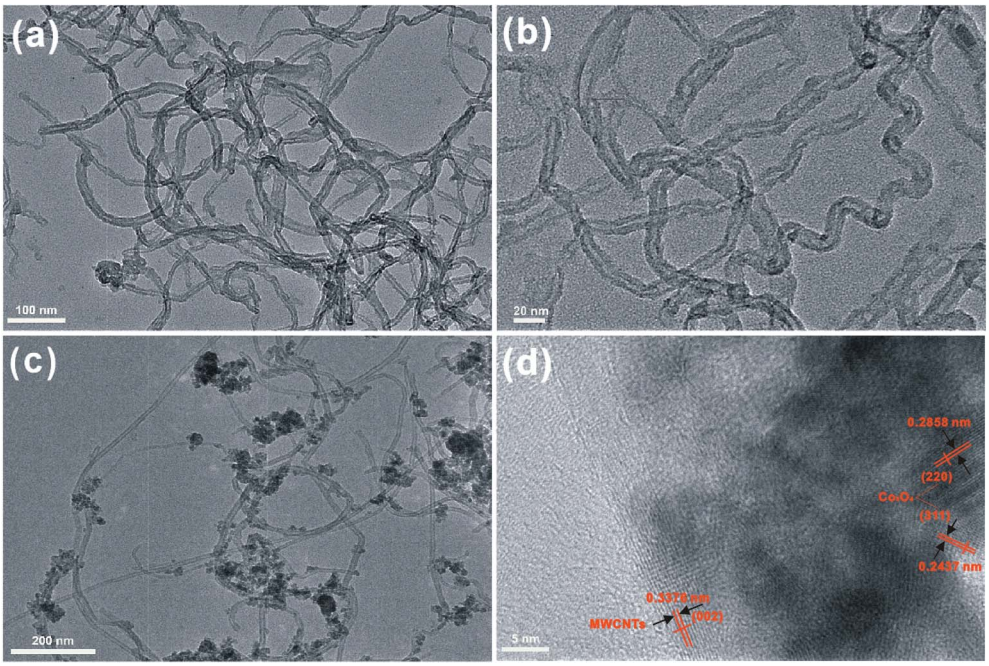

Fig. 2 (a and b) TEM images of MWCNTs, (c and d) TEM images of Co_3O_4/MWCNTs composites at various magnifications.

were successfully fabricate, without any other impurity phases.

MWCNTs and Co_3O_4/MWCNTs composites were further characterized using Raman spectroscopy in the range from 300 to 2000 cm^{-1}. In Fig. 1(b), the characteristic sharp D and G bands of carbon at around 1327 and 1590 cm^{-1} respectively were observed.[33–35] The I_D/I_G ratio was determined to be 1.25, indicating that the MWCNTs became disordered after being treated by concentrated HNO_3. Apart from the characteristic peaks of carbon materials (D and G bands), other four distinguishable peaks at 469, 522, 608, and 674 cm^{-1} appeared, which can be attributed to the E_g, F^1_{2g}, F^2_{2g}, and A_{1g} modes of crystalline Co_3O_4, respectively. Bare Co_3O_4 particles was also examined by Raman spectroscopy in the range from 400 to 700 cm^{-1}. As shown in Fig. 1(c), the four characteristic peaks of Co_3O_4 could be observed at 469, 522, 608, and 674 cm^{-1} as well. These Raman analysis data matched well with the XRD results.[36]

The morphology of Co_3O_4/MWCNTs composites were then investigated by FE-SEM analysis. Fig. 1(d) exhibits the SEM image of Co_3O_4/MWCNTs composites. It can be observed that the Co_3O_4 nanoparticles and MWCNTs mixed well with each other. The MWCNTs can work as a support, which increases the disperse of Co_3O_4 nanoparticles and prevent the agglomeration during usage. The MWCNTs could provide a conductive frame network for Co_3O_4 and consequently enhance its electrochemical properties. To show it more clearly, the morphologies of bare Co_3O_4 nanoparticles and pure MWCNTs were also explored and displayed in Fig. 1(e) and (f), respectively. The Co_3O_4 nanoparticles were in small size and the prepared MWCNTs were long in length and thin in diameter, and formed strong intertwined entanglements with a three-dimensional network structure.

The morphologies of MWCNTs and Co_3O_4/MWCNTs composites were also characterized using TEM analysis. The TEM images of MWCNTs with various magnifications indicate that MWCNTs were long and thin, with the diameter of nanotubes ranging from 8.0 to 11.3 nm, as shown in Fig. 2(a and b). Fig. 2(c) reveals that the Co_3O_4 nanoparticles were attached to the surface of MWCNTs. Fig. 2(d) shows the HR-TEM image of Co_3O_4 nanoparticles, in which the crystal lattice can be evidently observed. The lattice distance around 0.2858 and 0.2437 nm are corresponding to (220) and (311) planes of Co_3O_4, while the lattice distance around 0.3376 nm is concordant with (002) plane of MWCNTs. These results indicated the successful synthesis of Co_3O_4/MWCNTs composites.

To explore the porosity and the specific surface area of Co_3O_4/MWCNTs composites, the N_2 adsorption–desorption measurement was conducted. Fig. 3(a) exhibits an adsorption–desorption isotherm of typical V with an obvious H3 type hysteresis loop. Fig. 3(b) displays the pore size distribution curve, with one intense peak at 2.2 nm and another broad peak at around 15.1 nm. The former peak is attributed to Co_3O_4, while the latter is assigned to the multi-walled carbon nanotubes. The specific surface area of Co_3O_4/MWCNTs composite calculated by the Brunauer–Emmett–Teller (BET) method turns out to be197.8 $m^2\ g^{-1}$. The porous structure of Co_3O_4/MWCNTs facilitates the contact between active materials and electrolyte, inducing a faster transportation of the chemicals to be detected.

3.2 EIS study of Co_3O_4/MWCNTs GCE

The EIS technique was also employed to study the interfacial property of the prepared electrodes. The measurement was performed at the open circuit potential in 5 mM $[Fe(CN)_6]^{4-/3-}$ + 0.1 M KCl solution and the frequency was ranged from 1 to

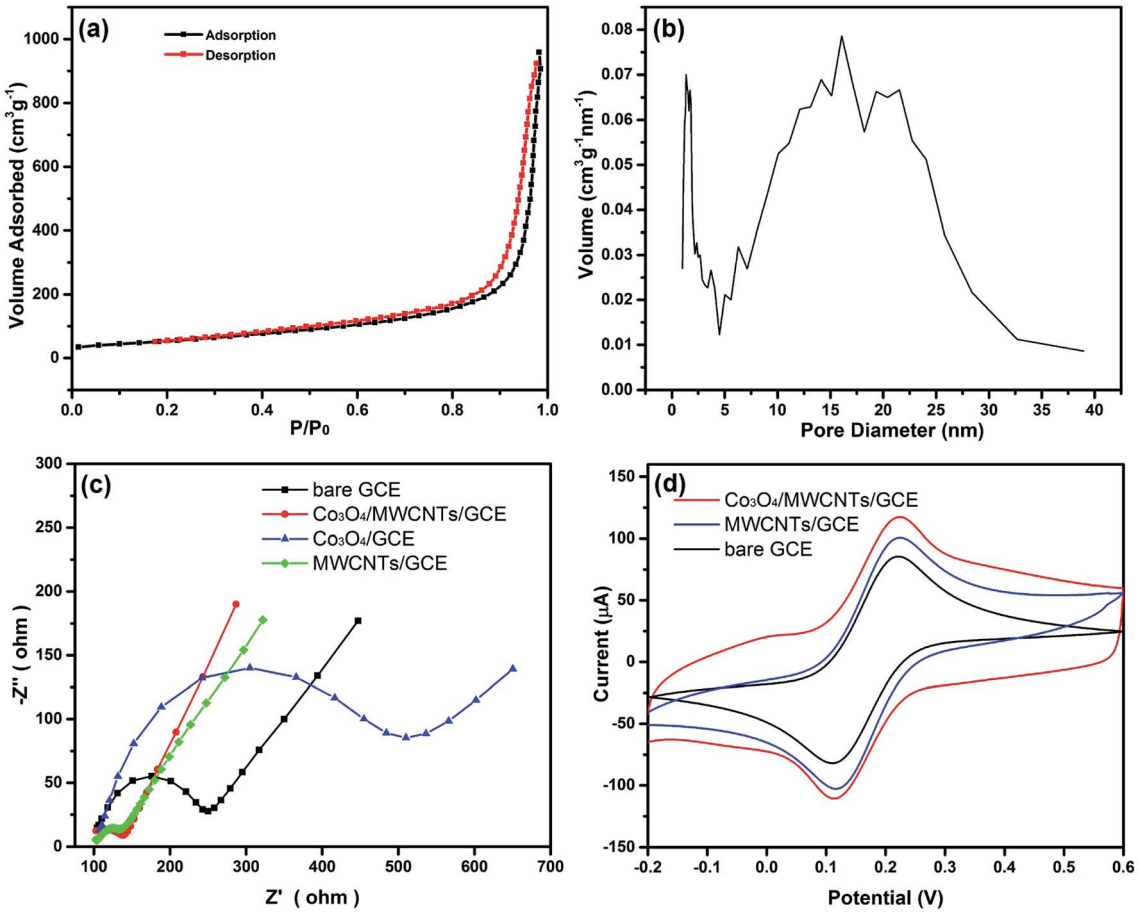

Fig. 3 (a) N_2 adsorption–desorption isotherm of Co_3O_4/MWCNTs composites, (b) the pore size distribution of Co_3O_4/MWCNTs composites, (c) electrochemical impedance spectroscopy of bare GCE, Co_3O_4/GCE, MWCNTs/GCE and Co_3O_4/MWCNTs/GCE in 5 mM of $[Fe(CN)_6]^{3-/4-}$ solution containing 0.1 M KCl, frequency: 1–100 KHz, (d) CV responses of bare GCE, MWCNTs/GCE, and Co_3O_4/MWCNTs/GCE in 0.1 M KCl electrolyte comprising 5 mM of $[Fe(CN)_6]^{3-/4-}$ at a scan rate of 0.05 V s^{-1}.

100 kHz with the potential amplitude of 5 mV. Fig. 3(c) demonstrates the Nyquist plot of the prepared electrodes. The bare GCE showed a high R_{ct} value of 200.6 Ω. The MWCNTs/GCE showed a rather low R_{ct} value of 56.9 Ω, suggesting the excellent conductivity of MWCNTs. When the GCE was modified with Co_3O_4, R_{ct} was increased to the value of 428.7 Ω, indicating the poor electrical conductivity of Co_3O_4. Modified with Co_3O_4/MWCNTs composites, the R_{ct} was significantly decreased to the value of 87.8 Ω, indicating the satisfactory electrical conductivity with the introduction of MWCNTs (Table 1). Compared with the large semicircles for bare GCE and Co_3O_4/GCE, the depressed semicircle of Co_3O_4/MWCNTs/GCE also validates high conductivity and fast electron conducting ability of the MWCNTs.[37] The $[Fe(CN)_6]^{3-/4-}$ was also requisite as the electrochemical probe to further explore the electroactive surface area of the prepared electrode. The study was conducted in 0.1 M KCl solution containing 5 mM $[Fe(CN)_6]^{3-/4-}$ at a scan rate of 0.05 V s^{-1}. Fig. 3(d) illustrates the CV responses of bare GCE, MWCNTs/GCE, and Co_3O_4/MWCNTs/GCE, all of them exhibited a pair of well-defined redox peaks which correspond to the $[Fe(CN)_6]^{3-/4-}$ redox couple. However, notably, the Co_3O_4/MWCNTs/GCE exhibited higher current response than MWCNTs/GCE or bare GCE, which may be due to the synergistic effect between MWCNTs and Co_3O_4. The high current response of Co_3O_4/MWCNTs/GCE also reveals that the electroactive surface area of the modified electrode has initiated an accelerating increase after the modification procedure. The large electroactive surface area of Co_3O_4/MWCNTs can provide more active sites and improve the probability for the contact with hydrazine.

3.3 Electrochemical determination of hydrazine

The as-fabricated Co_3O_4/MWCNTs composites were then applied in the electrochemical hydrazine detection, and the electrochemical performance towards the hydrazine detection was essentially implemented by the cyclic voltammetry (CV). Fig. 4(a) shows the CV curves of bare GCE, MWCNTs/GCE, Co_3O_4/GCE, and Co_3O_4/MWCNTs/GCE in the presence of 1 mM N_2H_4 in 0.1 M NaOH solution with a scan rate of 0.02 V s^{-1}. The electrocatalytic ability of MWCNTs/Co_3O_4/GCE is better than MWCNTs/GCE or Co_3O_4/GCE, manifesting the great synergistic effect which based on the outstanding catalytic activity of Co_3O_4 and high specific surface area of MWCNTs.[38]

Table 1 The charge transfer resistance (R_{ct}) values of different electrodes

Electrodes	R_{ct}
Bare GCE	200.6 Ω
Co_3O_4/GCE	428.7 Ω
Co_3O_4/MWCNTs/GCE	87.8 Ω
MWCNTs/GCE	56.9 Ω

For bare GCE, it is obvious that there was no redox peak in the potential range of 0 to 0.6 V, suggesting the poor electrochemical activity of GCE. The observed redox peaks of Co_3O_4/GCE and Co_3O_4/MWCNTs/GCE appeared at 0–0.6 V can be assigned to the reversible electron transfer of $CoOOH/CoO_2$.[39] Notably, the peak current of Co_3O_4/MWCNTs/GCE is about 50.18 μA, which is larger than the value of Co_3O_4/GCE (6.63 μA). The obtained results indicate that the prepared Co_3O_4/MWCNTs composites can be utilized for effective detection of hydrazine. The involved reaction can be illustrated as eqn (2) and (3). The Co_3O_4 cannot steadily exist in alkaline solution due to the interaction with OH^-, with the generation of CoOOH or even CoO_2.

$$Co_3O_4 + OH^- + H_2O \rightarrow 3CoOOH + e^- \quad (2)$$

$$CoOOH + OH^- \rightarrow CoO_2 + H_2O + e^- \quad (3)$$

With addition of hydrazine, the oxidation of hydrazine and the reduction of CoO_2 occurs simultaneously. CoO_2 as an intermediate can produce CoOOH, which increases the quantity of CoOOH for further oxidation, leading to an increased anodic current (eqn (4)).

$$4CoO_2 + N_2H_4 \rightarrow 4CoOOH + N_2 \quad (4)$$

To evaluate the electrochemical kinetics of the Co_3O_4/MWCNTs modified electrode, the effect of scan rate on the oxidation peak current along with the peak potential has also been investigated, respectively. Fig. 4(b) presents the cyclic voltammogram of the Co_3O_4/MWCNTs modified electrode at scan rates ranging from 0.01 V s^{-1} to 0.1 V s^{-1} with the addition

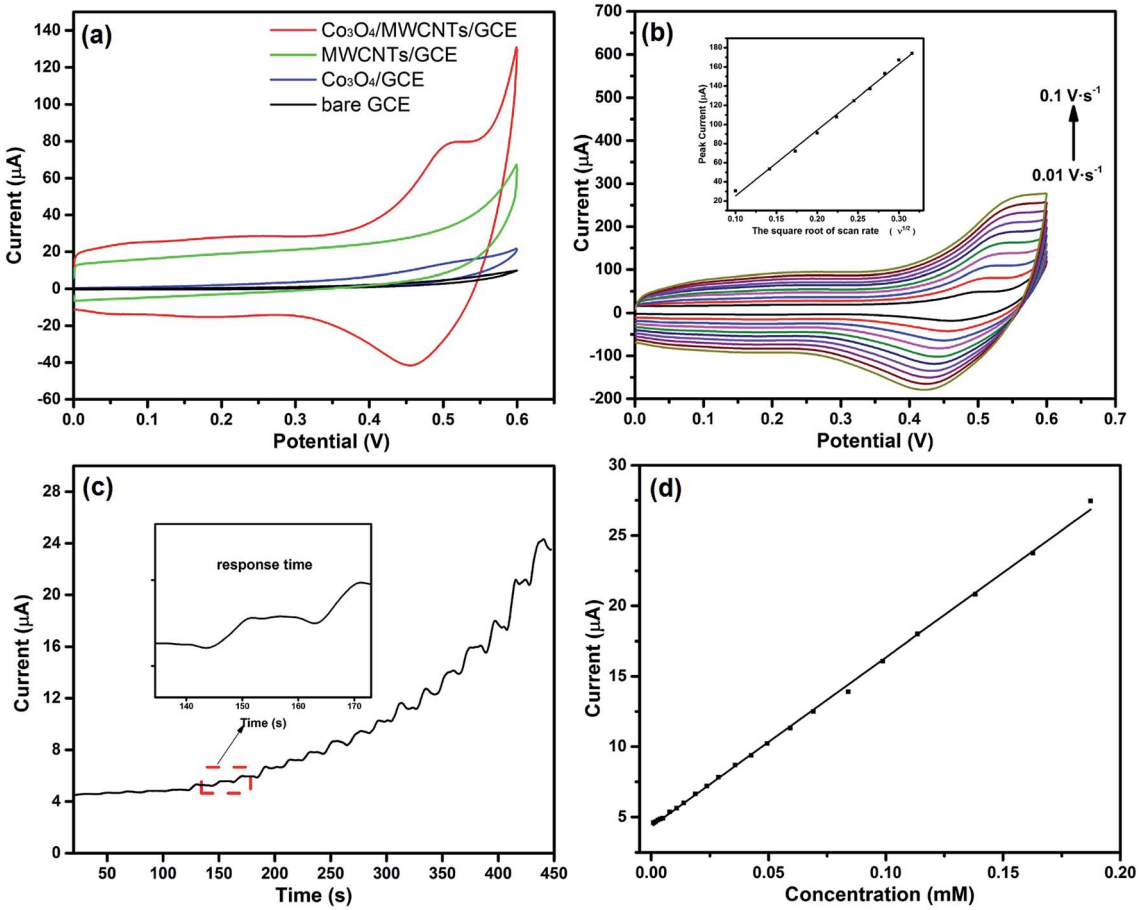

Fig. 4 (a) Cyclic voltammograms of bare GCE, MWCNTs/GCE, Co_3O_4/GCE, and Co_3O_4/MWCNTs/GCE in the presence of 1 mM N_2H_4 in 0.1 M NaOH solution with a scan rate of 0.02 V s^{-1}, (b) cyclic voltammogram of the Co_3O_4/MWCNTs/GCE at different scan rates (from 0.01 to 0.1 V s^{-1}), and the inset shows the anodic peak current *vs.* square root of scan rate ($\nu^{1/2}$), (c) amperometric response of Co_3O_4/MWCNTs/GCE towards the step injection of hydrazine and the inset shows the response time after successive addition of hydrazine, (d) the linear relationship between the response current and the hydrazine concentration.

Table 2 Analytical parameters for hydrazine detection based on Co_3O_4 and Co_3O_4/MWCNTs composites modified electrodes

Electrode materials	Sensitivity ($\mu A\ mM^{-1}$)	Detection limit (μM)	Linear range (μM)	Response time (s)	Reference
Co_3O_4 nanoparticle	22.20	2.80	20–400	—	47
Co_3O_4 nanowire	28.60	0.50	20–700	<6	47
Chrysanthemum-like Co_3O_4	107.89	5.87	50–1088	<10	48
Urchin-shaped Co_3O_4	76.31	1.29	5–610	—	49
Co_3O_4 nanoneedle bundle	95.25	2.93	5–446	<8	49
Co_3O_4/MWCNTs composite	120.26	0.449	1–187.4	<5	This work

of 1 mM N_2H_4 in 0.1 M NaOH solution. Interestingly, a pair of redox peaks corresponding to the reversible transition between CoOOH and CoO_2 was distinctly observed. Moreover, the oxidation peak presented a small and gradual shift, and the peak current intensity elevated gradually with increasing scan rates. The oxidation peak currents are directly proportional to the square root of the scan rate up to 0.1 V s^{-1}, as shown in the inset of Fig. 4(b). The linear equations can be defined as $I_p = 688.33\nu^{1/2}$ (V s^{-1}) − 43.52 ($R^2 = 0.996$). The negative intercept reveals that the electrode reaction is not a single diffusion-controlled process. The negative intercept from the plot of the peak current *versus* the square root of the scan rate can be explicated as the adsorption of the N_2H_4 molecule after diffusion to the electrode surface.[40] The total number of electrons involved in the reaction process can be calculated by the Randles–Sevick equation, as shown in eqn (5),[41,42] where I_p represents the oxidation peak current, n represents the number of electrons participating in the redox reaction, A refers to the electroactive surface area of the electrode (cm^2), D refers to the diffusion coefficient of hydrazine in the solution ($cm^2\ s^{-1}$), C is the concentration of hydrazine in the bulk solution (mol cm^{-3}), and ν represents the scan rate (V s^{-1}). The number of electron transfer was found out to be 4 corresponding to the reaction eqn (6).

$$I_p = (2.69 \times 10^5)n^{3/2}AD^{1/2}C\nu^{1/2} \quad (5)$$

$$N_2H_4 + 4OH^- \rightarrow N_2 + 4H_2O + 4e^- \quad (6)$$

To further investigate the sensing performance, amperometric response of the fabricated hydrazine sensor is conducted at 0.502 V. Fig. 4(c) shows that the current curve displays a constructive promotion and reaches 95% of the steady-state current in less than 5 s upon the addition of hydrazine step by step. The response is much faster than the reported Co_3O_4/GCE (Table 2). The fast current response may be attributed to the conductive frame network provided by MWCNTs. The produced electron can transfer more easily and the diffusion of reactants can be enhanced as well in the presence of MWCNTs. Fig. 4(d) shows the typical corresponding calibration of the hydrazine concentrations *versus* current in a wide liner range from 1.0 μM to 187.4 μM. Notably, the low concentration points can be well fitted with the high concentration points. The linear regression equation can be described as I_p (μA) = 120.26C (mM) + 4.313 ($R^2 = 0.999$). The sensitivity attained from the slope is found to be 120.26 $\mu A\ mM^{-1}$. The high electrocatalytic response observed from Co_3O_4/MWCNTs correlates well with the large specific surface area, tremendous site accessibility and low mass-transfer resistance for hydrazine.

To calculate the limit of detection (LOD), the standard approach recommended by International Union of Pure and Applied Chemistry (IUPAC) is utilized, as shown in eqn (7), where N is the noise of the blank solution and S represents the slope of the calibration curve. The detection limit is calculated to be 0.449 μM. A summary of the Co_3O_4 modified electrodes towards the electrocatalytic oxidation of hydrazine is listed in Table 2. It is noteworthy that the introduction of MWCNTs greatly enhanced the sensitivity and relatively lowered the detection limit which may be abscribed to the synergic effect between Co_3O_4 and MWCNTs towards the electrooxidation of hydrazine.

$$LOD = 3N/S \quad (7)$$

Selectivity is another key factor to measure the sensor performance. Hydrazine, as one of strong reducing agents, is widely used as an oxygen scavenger for corrosion control in boilers and hot-water heating systems.[43] In the wastewater of boilers and hot-water heating systems, Na^+, SO_4^{2-}, K^+, NO_3^-, NH_4^+, Cl^-, and tap water are parts of the most common compositions.[44] These compositions are considered as the

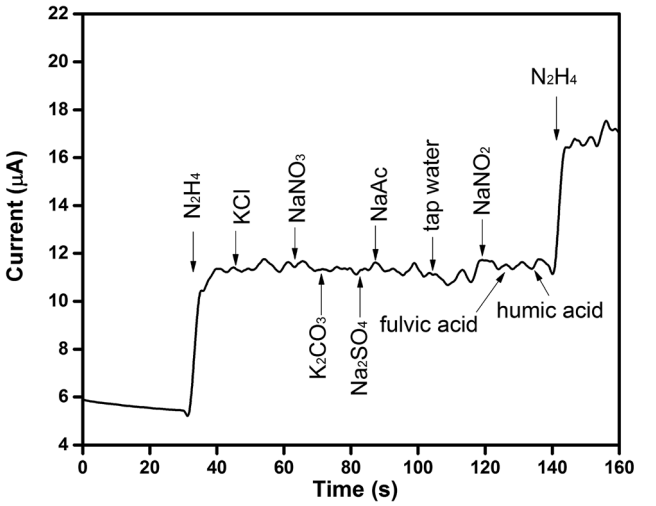

Fig. 5 The amperometric response to the introduction of hydrazine with interfering species.

interferents that may affect the detection of hydrazine.[45] In this work, besides these inorganic interferents, other active chemicals such as NO_2^-, fulvic acid and humic acid were also used to test the selectivity of the fabricated Co_3O_4/MWCNTs/GCE towards hydrazine. Fig. 5 illustrates the amperometric responses of Co_3O_4/MWCNTs modified electrode to hydrazine with interferents, including K^+, Cl^-, Na^+, SO_4^{2-}, CO_3^{2-}, Ac^-, NO_3^-, tap water, NO_2^-, fulvic acid, and humic acid. The responses to inorganic interfering species were investigated by continuously adding 10 μL (0.1 M) of each interferent into the testing solution. It's obvious that the introduction of these interferents in the measuring solution did not bring any significant variation compared with the quick current response of hydrazine. On the other hand, the addition of 10 μL (0.1 M) reactive chemicals, such as NO_2^-, fulvic acid and humic acid, also shows negligible variation. These results suggest that the Co_3O_4/MWCNTs composites based sensor possesses good selectivity for hydrazine detection.

3.4 Electrochemical determination of glucose

The prepared Co_3O_4/MWCNTs hybrid materials were also applied for the electrocatalytic glucose determination. Fig. 6(a) illustrates the cyclic voltammogram of the bare GCE, Co_3O_4/GCE, and Co_3O_4/MWCNTs/GCE in the presence of 1 mM glucose in 0.1 M NaOH solution with a scan rate of 0.02 V s^{-1}. In the potential range from 0 to 0.6 V, just Co_3O_4/GCE and Co_3O_4/MWCNTs/GCE show a distinct oxidation peak at 0.518 V. It's also obvious that Co_3O_4/MWCNTs/GCE exhibits larger current response than Co_3O_4/GCE. The value of the oxidation peak current is up to 92.38 μA, which is 10 times larger than the current response of Co_3O_4/GCE. This result demonstrates that the hybrid material might provide potential applications for the electroactive oxidation of glucose. The corresponding chemical reaction can be well explained by eqn (2), (3), and (8).

$$2CoO_2 + C_6H_{12}O_6\ (\text{glucose}) \rightarrow 2CoOOH + C_6H_{10}O_6\ (\text{gluconolactone}) \quad (8)$$

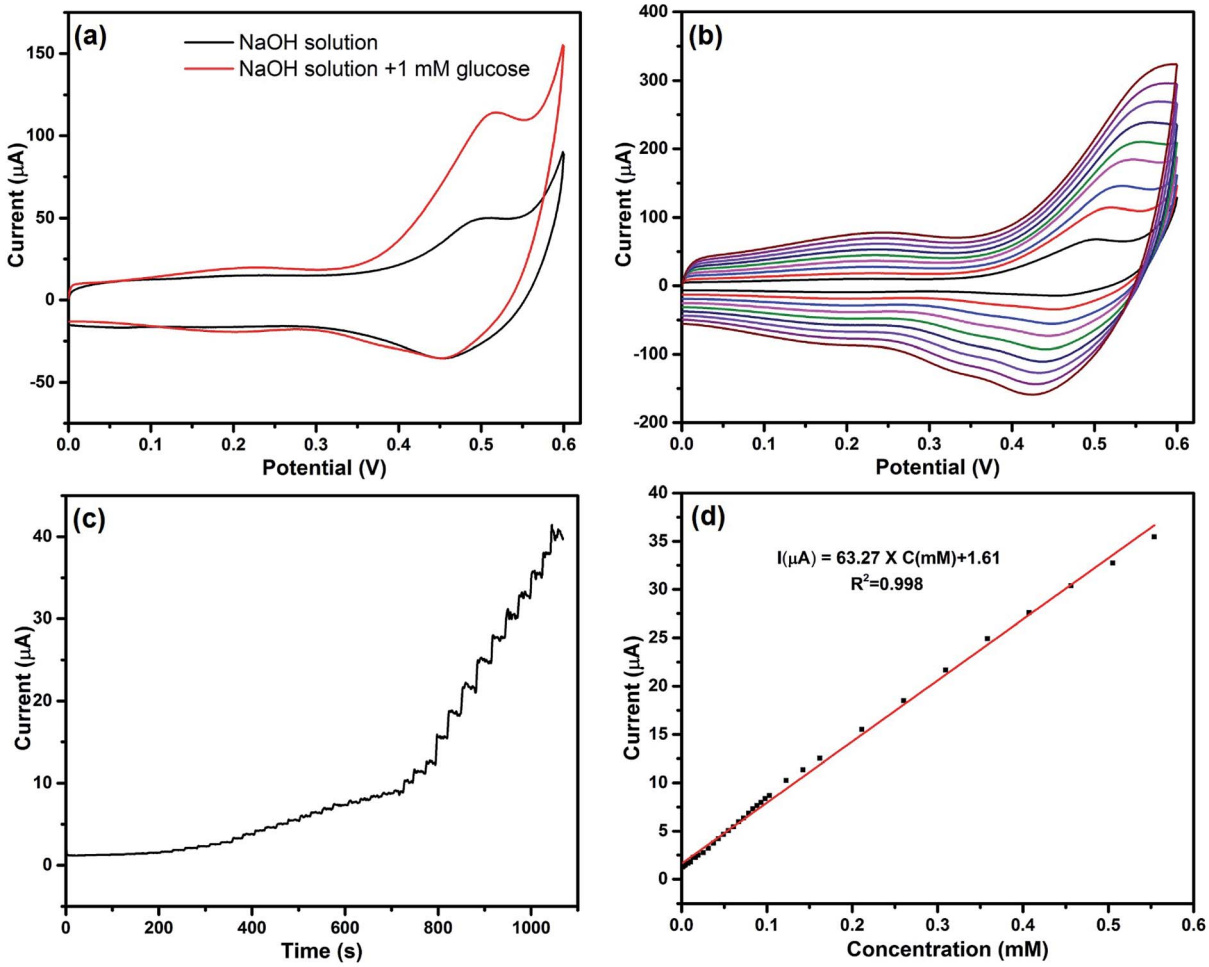

Fig. 6 (a) Cyclic voltammograms of Co_3O_4/MWCNTs/GCE in the presence and absence of 1 mM glucose in 0.1 M NaOH solution with a scan rate of 0.02 V s^{-1}, (b) cyclic voltammogram of the Co_3O_4/MWCNTs modified electrode at different scan rates (from 0.01 to 0.09 V s^{-1}), (c) amperometric response of Co_3O_4/MWCNTs/GCE towards the step injection of glucose, and (d) linear relationship between the response current and the glucose concentration.

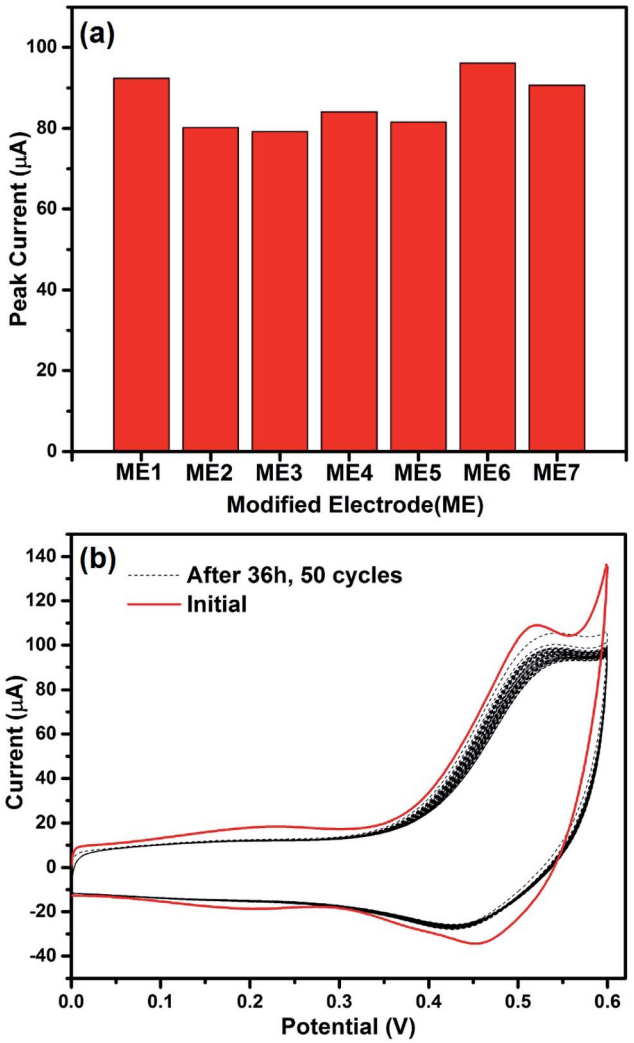

Fig. 7 (a) The peak currents of different modified electrodes, (b) CVs of the fresh modified electrode and Co_3O_4/MWCNTs/GCE after being stored in ambient air conditions for 36 h.

The investigation of the catalytic kinetic of glucose oxidation was then conducted by examining the impact of scan rate on the current response in the presence of 1 mM glucose. Fig. 6(b) shows that the oxidation peak currents were significantly elevated with increasing scan rates (from 0.01 to 0.09 V s^{-1}), implying that the oxidation of glucose is a surface-controlled electrochemical process.[46] The amperometric response of the Co_3O_4/MWCNTs/GCE for the successive addition of glucose at applied potential of 0.518 V was also recorded in detail. Fig. 6(c) exhibits the amperometric response of Co_3O_4/MWCNTs towards the step injection of glucose. The oxidation peak current was increased linearly with elevating glucose concentration in the range of 1.70–554 μM (Fig. 6(d)) with a correlation coefficient of 0.998. The detection limit calculated by the abovementioned method turns out to be 0.95 μM and the sensitivity obtained from the slope is found to be 63.27 μA mM^{-1}.

To estimate the reproducibility of the modified electrodes, seven electrodes (denoted as ME1 to ME7) were prepared in parallel. Fig. 7(a) demonstrates the peak currents of these seven modified electrodes measured at 0.518 V. The relative standard deviation value is 7.73%. Meanwhile, the stability was studied subsequently by evaluating the peak current response of Co_3O_4/MWCNTs/GCE in 1 mM glucose solution after being stored in ambient air conditions for 36 hours. Fig. 7(b) shows that negligible difference can be observed even after 50 cycles. Moreover, after being stored for 36 hours, the peak current can still maintain 93.4% of its initial response. These results indicate that the fabricated glucose sensor is reproducible and quite stable.

4. Conclusion

Co_3O_4/MWCNTs composites have been successfully fabricated using a facile hydrothermal method and then applied as electron transfer mediator for hydrazine and glucose sensing. The structure and morphology of Co_3O_4/MWCNTs composites were carefully characterised, which indicated that the Co_3O_4 nanoparticles were homogeneously attached on the surface of MWCNTs. The EIS study demonstrated that Co_3O_4/MWCNTs/GCE exhibited higher conductivity than bare GCE and Co_3O_4/GCE, endorsing a faster electron transfer rate and a higher electrocatalytic activity. The comprehensive sensing results indicated that the fabricated Co_3O_4/MWCNTs composites possessed high electrocatalytic activity for the detection of hydrazine and glucose. After doping on GCE, the fabricated Co_3O_4/MWCNTs/GCE sensor displayed an ultra-high sensitivity of 120.26 μA mM^{-1}, a rather low detection limit of 0.449 μM, and a wide linear range of 1–187.4 μM for the detection of hydrazine. This Co_3O_4/MWCNTs/GCE sensor also showed a high sensitivity of 63.27 μA mM^{-1}, a low detection limit of 0.95 μM, and a wide linear range of 1.70–554 μM for glucose detection. In all, we demonstrated that the fabricated Co_3O_4/MWCNTs composites have promising application prospects in the construction of effective detection of hydrazine and glucose.

Conflicts of interest

There are no conflicts to declare.

Acknowledgements

This work was supported by the Fundamental Research Funds for the Central Universities (2016ZCQ03), the National Natural Science Foundation of China (51622801, 51572029), and the Beijing Excellent Young Scholar (2015000026833ZK11). Ahmad Umar would like to acknowledge the Ministry of Higher Education, Kingdom of Saudi Arabia for the research grant (PCSED-001-11) under the Promising Centre for Sensors and Electronic Devices (PCSED) at Najran University.

References

1 T. Zhou, Q. Wang, A. Umar, F. Xu, Y. Gao, J. Wu, Z. zhang, Y. Yang, J. Wang, L. Huang, P. Lu and Z. Guo, *Sci. Adv. Mater.*, 2015, 7, 2069–2083.

2 E. Comini, C. Baratto, I. Concina, G. Faglia, M. Falasconi, M. Ferroni and D. Zappa, *Sens. Actuators, B*, 2013, **179**, 3–20.
3 X. W. Lou, C. M. Li and L. A. Archer, *Adv. Mater.*, 2009, **21**, 2536–2539.
4 H. Gao, F. Xiao, C. B. Ching and H. Duan, *ACS Appl. Mater. Interfaces*, 2012, **4**, 2801–2810.
5 P. G. Freire, R. H. Montes, F. C. Romeiro, S. C. Lemos, R. C. Lima, E. M. Richter and R. A. Munoz, *Sensor Actuat. B: Chem.*, 2016, **223**, 557–565.
6 A. Gulino, G. Fiorito and I. Fragalà, *J. Mater. Chem.*, 2003, **13**, 861–865.
7 Q. Jiao, M. Fu, C. You and Y. Zhao, *Inorg. Chem.*, 2012, **51**, 11513–11520.
8 H. Lu, C. Jiang, Z. Ding, W. Wang, W. Chu and Y. Feng, *J. Energy Chem.*, 2016, **25**, 387–392.
9 Y. Ren, S. Zhang, H. Fang, X. Wei and P. Yang, *J. Energy Chem.*, 2014, **23**, 801–808.
10 L. Yao, H. Zhong, C. Deng, X. Li and H. Zhang, *J. Energy Chem.*, 2016, **25**, 153–157.
11 J. Xu, P. Gao and T. S. Zhao, *Energy Environ. Sci.*, 2012, **5**, 5333–5339.
12 X. H. Xia, J. P. Tu, Y. J. Mai, X. L. Wang, C. D. Gu and X. B. Zhao, *J. Mater. Chem. A*, 2011, **21**, 9319–9325.
13 X. Wang, X. Wu, B. Xu and T. Hua, *J. Solid State Electrochem.*, 2016, **20**, 1303–1309.
14 W. Eom, A. Kim, H. Park, H. Kim and T. H. Han, *Adv. Funct. Mater.*, 2016, **26**, 7605–7613.
15 C. Li, X. Yin, T. Wang and H. Zeng, *Chem. Mater.*, 2009, **21**, 4984–4992.
16 L. Zhuo, Y. Wu, J. Ming, L. Wang, Y. Yu, X. Zhang and F. Zhao, *J. Mater. Chem. A*, 2013, **1**, 1141–1147.
17 F. Zhang, C. Yuan, X. Lu, L. Zhang, Q. Che and X. Zhang, *J. Power Sources*, 2012, **203**, 250–256.
18 K. Jurewicz, K. Babeł, R. Pietrzak, S. Delpeux and H. Wachowska, *Carbon*, 2006, **44**, 2368–2375.
19 W. Tang, Y. Y. Hou, X. J. Wang, Y. Bai, Y. S. Zhu, H. Sun and R. Holze, *J. Power Sources*, 2012, **197**, 330–333.
20 X. Wang, M. Li, Z. Chang, Y. Yang, Y. Wu and X. Liu, *ACS Appl. Mater. Interfaces*, 2015, **7**, 2280–2285.
21 X. Wang, M. Li, Z. Chang, Y. Wang, B. Chen, L. Zhang and Y. Wu, *J. Electrochem. Soc.*, 2015, **162**, A1966–A1971.
22 A. M. El-Brashy and L. A. El-Hussein, *Synth. React. Inorg. Met.-Org. Chem.*, 1997, **30**, 609–622.
23 M. A. Eid, *Microchim. Acta*, 1998, **129**, 91–95.
24 A. L. de Toledo Fornazari, W. T. Suarez, H. J. Vieira and O. Fatibello-Filho, *Acta Chim. Slov.*, 2005, **52**, 164–167.
25 A. E. Katrusiak, P. G. Paterson, H. Kamencic, A. Shoker and A. W. Lyon, *J. Chromatogr. B*, 2001, **758**, 207–212.
26 M. Abdul Aziz and A. N. Kawde, *Talanta*, 2013, **115**, 214–221.
27 G. Wang, C. Zhang, X. He, Z. Li, X. Zhang, L. Wang and B. Fang, *Electrochim. Acta*, 2010, **55**, 7204–7210.
28 E. Zhang, Y. Xie, S. Ci, J. Jia and Z. Wen, *Biosens. Bioelectron.*, 2016, **81**, 46–53.
29 S. Garrod, M. E. Bollard, A. W. Nicholls, S. C. Connor, J. Connelly, J. K. Nicholson and E. Holmes, *Chem. Res. Toxicol.*, 2005, **18**, 115–122.
30 S. D. Zelnick, D. R. Mattie and P. C. Stepaniak, *Aviat., Space Environ. Med.*, 2003, **74**, 1285–1291.
31 K. Yamada, K. Yasuda, N. Fujiwara, Z. Siroma, H. Tanaka, Y. Miyazaki and T. Kobayashi, *Electrochem. Commun.*, 2003, **5**, 892–896.
32 X. Yue, W. Yang, M. Xu, X. Liu and J. Jia, *Talanta*, 2015, **144**, 1296–1300.
33 A. C. Ferrari and J. Robertson, *Phys. Rev. B*, 2000, **61**, 14095–14107.
34 X. Dong, B. Li, A. Wei, X. Cao, M. B. Chan-Park, H. Zhang, L. J. Li, W. Huang and P. Chen, *Carbon*, 2011, **49**, 2944–2949.
35 J. S. Cho, Y. J. Hong and Y. C. Kang, *ACS Nano*, 2015, **9**, 4026–4035.
36 B. Fang, C. Zhang, W. Zhang and G. Wang, *Electrochim. Acta*, 2009, **55**, 178–182.
37 M. A. Prathap, S. Sun and Z. Xu, *RSC Adv.*, 2016, **6**, 22973–22979.
38 G. Huang, F. Zhang, X. Du, Y. Qin, D. Yin and L. Wang, *ACS Nano*, 2015, **9**, 1592–1599.
39 Y. Ding, Y. Wang, L. Su, M. Bellagamba, H. Zhang and Y. Lei, *Biosens. Bioelectron.*, 2010, **26**, 542–548.
40 M. A. Prathap, S. Sun, C. Wei and Z. Xu, *Chem. Commun.*, 2015, **51**, 4376–4379.
41 M. A. Prathap, V. Anuraj, B. Satpati and R. Srivastava, *J. Hazard. Mater.*, 2013, **262**, 766–774.
42 J. Wu, T. Zhou, Q. Wang and A. Umar, *Sensor Actuat. B: Chem.*, 2016, **224**, 878–884.
43 H. W. Schessl, in *Encyclopedia of Chemical Technology*, ed. K. Othmer, Wiley, New York, 4th edn, 1995, vol. 13, p. 560.
44 H. Karimi-Maleh, M. Moazampour, A. A. Ensafi, S. Mallakpour and M. Hatami, *Environ. Sci. Pollut. Res.*, 2014, **21**, 5879–5888.
45 J. Zhang, H. Liu, M. Dou, F. Wang, J. Liu, Z. Li and J. Ji, *Electroanalysis*, 2015, **27**, 1188–1194.
46 R. Madhu, V. Veeramani, S. M. Chen, A. Manikandan, A. Y. Lo and Y. L. Chueh, *ACS Appl. Mater. Interfaces*, 2015, **7**, 15812–15820.
47 J. Zhang, W. Gao, M. Dou, F. Wang, J. Liu, Z. Li and J. Ji, *The Analyst*, 2015, **140**, 1686–1692.
48 T. Zhou, P. Lu, Z. Zhang, Q. Wang and A. Umar, *Sensor Actuat. B: Chem.*, 2016, **235**, 457–465.
49 T. Zhou, C. Zhang, P. Lu, Z. Zhang, Y. Gao, Q. Wang and A. Umar, *Nanosci. Nanotechnol. Lett.*, 2016, **8**, 634–640.